Amorphous $Al_{90}Fe_xCe_{10-x}$ alloys: X-ray absorption analysis of the Al, Fe and Ce local atomic and electronic structures

A. N. Mansour*
Naval Surface Warfare Center, Carderock Division, Code 644, 9500 MacArthur Boulevard, West Bethesda, Maryland 20817-5700

A. Marcelli and G. Cibin
LNF, INFN Frascati, Italy

G. Yalovega, T. Sevastyanova, and A. V. Soldatov
Faculty of Physics, Rostov State University, 5 Sorge, Rostov-na-Donu, 344090, Russia
(Received 31 October 2001; published 22 March 2002)

X-ray-absorption fine structure (XAFS) above the Fe *K* edge, the Ce L_3 edge, and the Al *K* edge in amorphous $Al_{90}Fe_xCe_{10-x}$ ($x=3$, 5, and 7) alloys have been measured and analyzed. Quantitative analyses of the Fe *K*-edge and Ce L_3-edge extended XAFS spectra are limited to local structure parameters of the first coordination sphere. Comparison of experimental x-ray-absorption near-edge structure (XANES) spectra with theoretical multiple-scattering (MS) XANES spectra for model compounds, such as crystalline $FeAl_6$ and $CeAl_4$, allows one to determine the local structure around the aluminum, iron, and Ce sites in ternary amorphous alloys. Using the theoretical MS approach, we show that the Fe and Al *K*-edge XANES are sensitive to the structure of coordination spheres, which extend up to nearly 4.4 and 3.3 Å, respectively. The Ce L_3-edge XANES, on the other hand, is sensitive to the structure that extends up to 3.15 Å.

DOI: 10.1103/PhysRevB.65.134207 PACS number(s): 61.10.Ht, 61.43.−j, 71.23.−k

I. INTRODUCTION

Liquid-quenched amorphous $Al_{90}Fe_xCe_{10-x}$ ($x=3$, 5, and 7) alloys combine the properties of a metal with the short-range order of a glass.[1] Their structural characteristics led to a number of remarkable mechanical,[2] magnetic,[3] and corrosion[4,5] properties. These alloys have high strength, high ductility, low density, and high resistance to corrosion. A fundamental understanding of the atomic structure and electronic nature of these alloys is essential in order to explore the origin of their properties. Hence, the structure of these alloys was investigated by pulsed neutron and x-ray scattering methods.[1] The structure around the Fe and Ce sites of vapor-quenched amorphous $Al_{100-2x}Co_xCe_x$ ($x=8-10$) and $Al_{80}Fe_{10}Ce_{10}$ alloys was investigated by x-ray-absorption fine-structure (XAFS) analysis.[6] So far, to our best knowledge, XAFS local geometry for Al in these alloys as well as details of the interaction between electronic states in the conduction band have not been studied. It has been shown that the density of Al electronic states in quasicrystalline $Al_{63}Cu_{25}Fe_{12}$ alloys is rather sensitive to the Al local atomic arrangements.[7] In this alloy, the Al *p-d* states interact with the transition-metal *d* states near the Fermi level. For closely related decagonal $Al_{65}Cu_{15}Co_{20}$ and $Al_{70}Co_{15}Ni_{15}$ quasicrystals, the Al *p* states overlap with the nickel and cobalt *s* and *d* states in the conduction band and form significant pseudogaps in the Al $3p$ and $3s$ *d* states near the Fermi level.[8]

X-ray-absorption near-edge structure (XANES) spectroscopy at the Al *K* edge provides a unique tool for studying the density of Al unoccupied electronic *p* states.[9] The above-mentioned sensitivity of the unoccupied Al *p* states with regard to local geometry leads to the fact that the Al *K*-edge XANES differs significantly from one compound to another.[10] But in order to extract the necessary information from the experimental spectra one needs to perform a theoretical analysis of the Al *K*-edge XANES data. In a study of the geometry and electronic structure of aluminum silicates and oxides on the basis of analysis of the Al *K*-edge XANES, Cabaret *et al.*[11] showed that a full multiple-scattering approach is one of the most successful methods for theoretical analysis. In the present investigation, the Fe and Al *K*-edge, and the Ce L_3-edge XAFS spectra of amorphous $Al_{90}Fe_xCe_{10-x}$ ($x=3$, 5, and 7) alloys have been measured and analyzed. The goal is to determine the best model for the local structures of Al, Fe, and Ce in the $Al_{90}Fe_xCe_{10-x}$ system and to study the peculiarities of the electronic structure of these alloys using XAFS analysis. Fourier transforms of the Fe *K*- and Ce L_3-edge extended XAFS (EXAFS) spectra (not shown here) display prominent contributions from the first coordination spheres of Fe and Ce, respectively, with no significant contributions from higher coordination spheres due to the amorphous nature of these alloys. Hence, quantitative analyses of EXAFS spectra are limited to the first coordination spheres of Fe and Ce (Table I). The local structure parameters for Fe are independent of the composition range investigated here. Fe is coordinated with approximately 6.6 Al atoms at a distance of 2.46 Å. The disorder for the Fe-Al sphere is within the range expected for crystalline materials, such as those for metallic Cu and Fe.[12] The Ce-Al coordination sphere, on the other hand, consists approximately of 14 Al atoms at a distance that increased from 3.13 to 3.18 Å in going from $x=7$ to 3. The Ce-Al coordination is characterized by a high degree of structural disorder suggesting a distribution of Ce-Al distances in close proximity of each other. We have also included the structure parameters for crystalline (*c*) $Al_{90}Fe_3Ce_7$ for comparison purposes with amorphous (*a*) $Al_{90}Fe_3Ce_7$. Clearly, the Fe-Al distance increased from 2.46 to 2.56 Å in going from *a*-$Al_{90}Fe_3Ce_7$ to *c*-$Al_{90}Fe_3Ce_7$ without a significant change in the Fe-Al co-

TABLE I. Structure parameters for Fe and Ce as determined from analysis of the Fe *K*- and the Ce L_3-edge EXAFS spectra for amorphous (a) and crystalline (c) alloys. *N*, *R*, and σ^2 are the coordination number, distance, and mean-square relative displacement, respectively. *N* and σ^2 are accurate to $\pm 10\%$ and *R* to ± 0.02 Å. The *c*-$Al_{90}Fe_3Ce_7$ alloy was obtained by heating the *a*-$Al_{90}Fe_3Ce_7$ alloy.

Sample	*X*-*Y* pair	*N*	*R* (Å)	σ^2 (10^{-3} Å^2)
a-$Al_{90}Fe_7Ce_3$	Fe-Al	6.6	2.46	7.7
	Ce-Al	14.0	3.13	18.5
a-$Al_{90}Fe_5Ce_5$	Fe-Al	6.6	2.46	7.5
	Ce-Al	13.4	3.15	18.7
a-$Al_{90}Fe_3Ce_7$	Fe-Al	6.7	2.46	7.7
	Ce-Al	13.9	3.18	20.6
c-$Al_{90}Fe_3Ce_7$	Fe-Al	7.7	2.56	8.4
	Ce-Al	12.3	3.25	8.1

ordination and disorder. The Ce-Al distance increased from 3.18 to 3.25 Å in going from *a*-$Al_{90}Fe_3Ce_7$ to *c*-$Al_{90}Fe_3Ce_7$ without a significant change in coordination. However, the Ce-Al disorder decreased from 0.0206 to 0.0081 Å^2 in going from *a*-$Al_{90}Fe_3Ce_7$ to *c*-$Al_{90}Fe_3Ce_7$. Clearly, the Ce-Al environment has a higher degree of structural disorder relative to that of the Fe-Al environment only in the amorphous state. On the basis of the metallic state atomic radii [r(Al) $=1.43$, r(Fe)$=1.26$, and r(Ce)$=1.81$ Å], the anticipated Fe-Al and Ce-Al distances are estimated to be near 2.69 and 3.24 Å, respectively. Clearly, the observed Fe-Al and Ce-Al distances in the amorphous state are significantly less than those estimated on the basis of the atomic radii. This is also true in the case of the Fe-Al distance for *c*-$Al_{90}Fe_3Ce_7$. The observed Ce-Al distance for *c*-$Al_{90}Fe_3Ce_7$, on the other hand, is close to that of the Ce-Al distance anticipated on the basis of the metallic state atomic radii.

Hence, the objective is to explore the XANES regions for the Al and Fe *K* edges and the Ce L_3 edge and determine if additional structural information with regard to higher coordination spheres can be obtained on the basis of multiple-scattering (MS) analysis. The MS approach used in the present investigation has been successfully applied to interpret a large number of XANES spectra for various materials.[13–18] The analysis has been found rather powerful for the case of ordered alloys like Ni_3Al and $NiAl_3$,[19] but no such analysis has been applied to the study of amorphous $Al_{90}Fe_xCe_{10-x}$ alloys. We show that analysis of XANES data enabled us to select a suitable structural model including symmetry for the alloys investigated.

II. EXPERIMENT AND METHOD OF CALCULATION

Amorphous samples in the form of 25-μm thick ribbons with nominal compositions $Al_{90}Fe_xCe_{10-x}$ ($x=3$, 5, and 7) were prepared by rapid solidification from the liquid phase.[20] The room-temperature Fe *K*- and Ce L_3-edge XAFS spectra were measured in the transmission mode on beamline X-11A at the National Synchrotron Light Source. Details of the experimental setup were published elsewhere.[5] The energy resolution in the measured energy range is about 1.0 eV.

X-ray-absorption spectra near the Al *K* edge were measured at the Jumbo beamline (BL3-3) of the Stanford synchrotron-radiation laboratory with Stanford positron electron accelerator ring (SPEAR) operating at an electron energy of 3 GeV and an injection current near 100 mA. Room-temperature spectra were collected in the total electron yield mode using a $YB_{66}(400)$ double-crystal monochromator with an energy resolution of about 0.6 eV. Energy calibration was done relative to pure aluminum foil. Spectra were corrected taking into account the variations of the current in the storage ring.

The algorithm of the scattering wave method was described earlier.[16] The local structure around the iron and cerium sites for the family of $Al_{90}Fe_xCe_{10-x}$ ternary alloys was treated using structural models based on the structure of crystalline $FeAl_6$,[21] $CeAl_4$,[21] and $FeAl_3$ (Ref. 22) binary alloys. Fe in $FeAl_3$ has five nonequivalent sites. In this case, the theoretical spectrum represents the weighted average of contributions from all nonequivalent sites. The theoretical spectra for Fe were calculated using actual atomic distances for crystalline $FeAl_6$ and crystalline $FeAl_3$ as well as those for $FeAl_6$ reduced by 3.4% (see Table II). The theoretical spectra for Ce were calculated using actual atomic distances for crystalline $CeAl_4$ as well as those reduced by 6% (Table III). To study the local geometry around the Al atoms, the theoretical spectra were calculated using actual atomic distances in crystalline $FeAl_3$ and crystalline $FeAl_6$ as well as those for crystalline $FeAl_6$ reduced by 3.4%.

Phase shifts of the photoelectrons were calculated in the framework of the crystal muffin-tin (MT) potential scheme with touching MT spheres. The MT radii and constants were obtained according to an established procedure of MT potential construction.[16] The MT approximation according to the Mattheiss prescription with the exchange parameter equal to 1.0 was used while constructing the crystal potential. Atomic

TABLE II. Structure parameters for Fe in crystalline $FeAl_6$ with interatomic distances reduced by 3.4% from the actual ones.

Shell number	Number and type	Shell radii (Å)
1	10 Al	2.460
2	10 Al	4.061
3	6 Al	4.379

TABLE III. Structure parameters for Ce in crystalline Al_4Ce with interatomic distances reduced by 6% from the actual ones.

Shell number	Number and type	Shell radii (Å)
1	16 Al	3.141
2	2 Al	3.577
3	4 Ce	4.112

charge densities were obtained with the help of a self-consistent Dirac-Slater method.

It is well known[23] that within the dipole approximation the x-ray-absorption coefficient, $\alpha(E)$, for the Fe K edge, is given by

$$\alpha(E) \sim |m_L(E)|^2 N_p^{\mathrm{Fe}}(E), \tag{1}$$

where $N_p^{\mathrm{Fe}}(E)$ is the partial density of unoccupied Fe states with p symmetry and $m_L(E)$ is the normalized dipole transition matrix element given by

$$m_L(E) = \frac{\int dr \phi_l(r,E) \Delta(r) \Psi_c(r)}{\left[\int dr \Phi_l^2(r,E)\right]^{1/2}}, \tag{2}$$

where $\Phi_l(r,E)$ is a solution of the radial Schrödinger equation at energy E for the MT potential ($l=1$ for the K edge), $\Delta(r)$ is the electron-photon interaction operator, and $\Psi_c(r)$ is the core K-level wave function. In the calculation, phase shifts with orbital momentum (l) up to 4 have been included even though there is almost no change in the spectra when compared with those calculated with l up to 2. For the Ce L_3-edge XANES, the situation is more complicated. There are two dipole allowed channels ($p \rightarrow d$ and $p \rightarrow s$), so the Ce XANES corresponds to the density of unoccupied states with s and d symmetries. However, the transition matrix element for the $p \rightarrow s$ transition is about 50 times smaller than that for the $p \rightarrow d$ transition. Hence, it is sufficient to take into account only the contribution of the $p \rightarrow d$ transition.

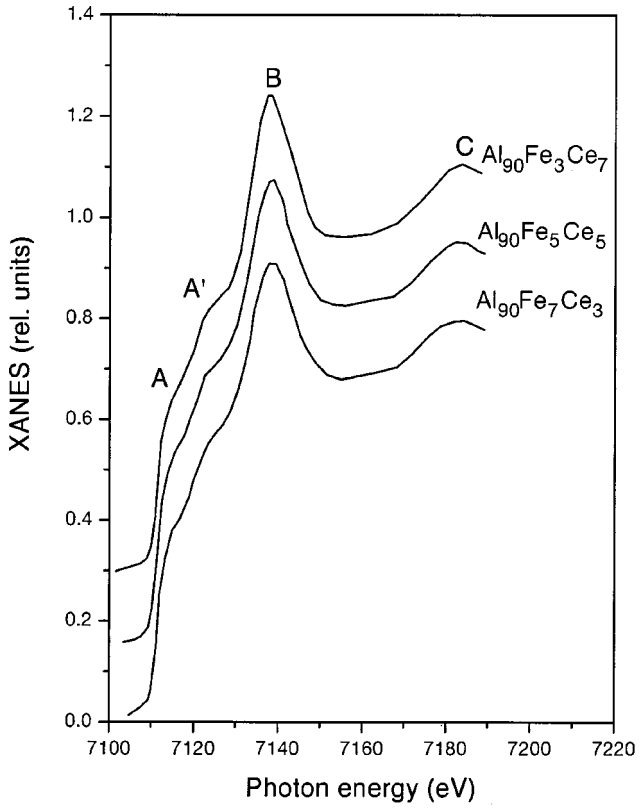

FIG. 1. Experimental Fe K-edge XANES in amorphous $Al_{90}Fe_xCe_{10-x}$ ($x=3$, 5, and 7) alloys.

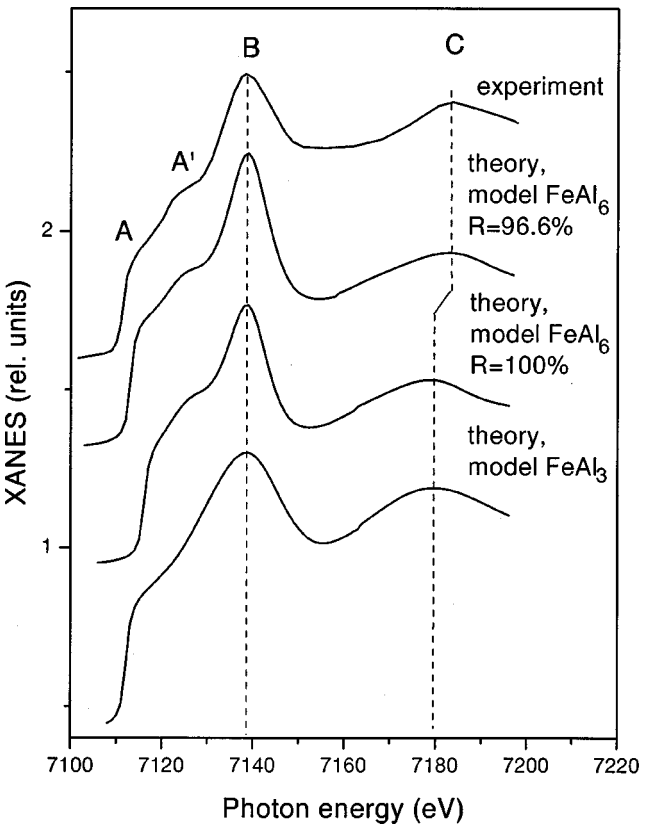

FIG. 2. Experimental Fe K-edge XANES for a-$Al_{90}Fe_3Ce_7$ compared with theoretical XANES for model compounds: crystalline $FeAl_3$, $FeAl_6$, and $FeAl_6$ with distances reduced by 3.4%.

In order to perform a direct comparison with experimental data one must take into account two factors. One factor is the filling of the occupied states following the Fermi distribution. The other factor is the broadening of experimental spectra due to the core hole lifetime, the finite mean free path of the photoelectron, and the experimental resolution. For the bandwidth of the core hole, 1.25 eV for the Fe K-edge XANES, 0.42 eV for the Al K-edge XANES, and 3.48 eV for the Ce L_3-edge XANES were used.[24] The energy-dependent function obtained by Muller, Jepsen, and Wilkins[23] was used for the mean free path of the photoelectron. For the experimental energy resolution a value of 1.0 eV was used for the Fe K- and the Ce L_3-edge XANES while a value of 0.6 eV was used for the Al K-edge XANES. These factors were treated as contributions to the imaginary part of the self-energy term.

In addition, one must compare the experimental data with

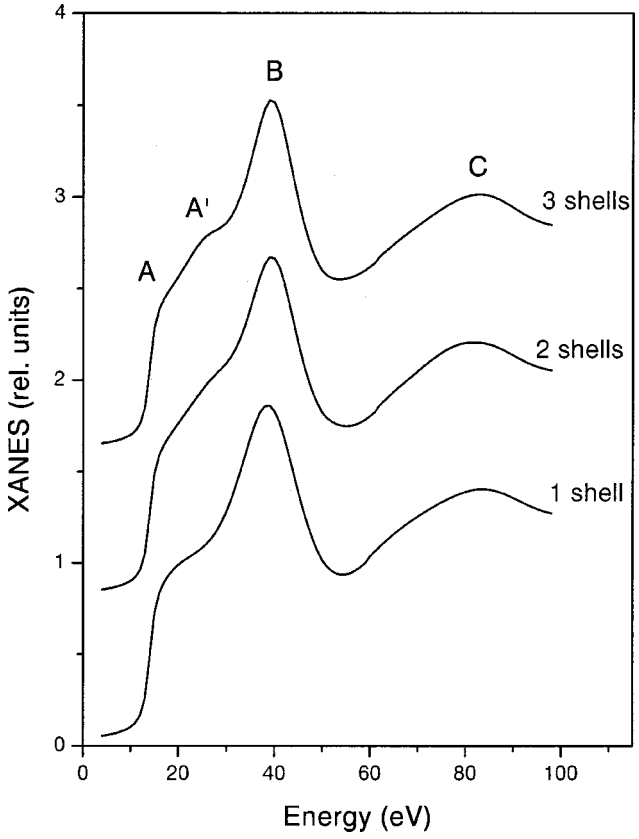

FIG. 3. Theoretical Fe *K*-edge XANES spectra calculated as a function of cluster size using structure data for crystalline $FeAl_6$ with atomic distances reduced by 3.4%. Origin of the energy scale corresponds to the zero of the MT potential.

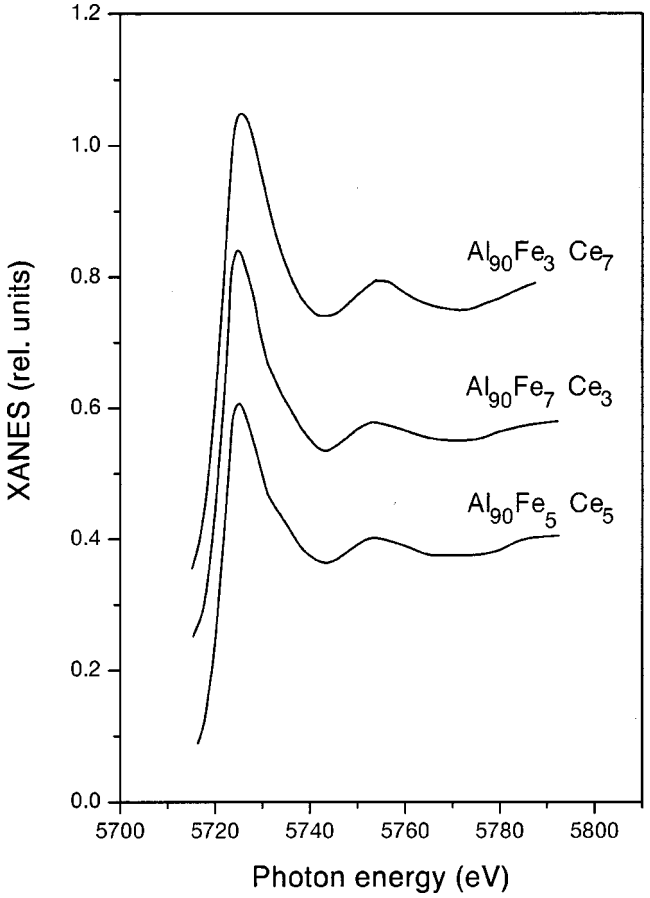

FIG. 4. Experimental Ce L_3-edge XANES for amorphous $Al_{90}Fe_xCe_{10-x}$ ($x=3$, 5, and 7) alloys.

the theoretical calculation made using a relaxed potential (i.e., taking into account the presence of the core hole). This effect was treated in the $Z+1$ approximation[13] and it was found that for the *K* edge the contribution of the core hole is rather small, while for the Ce L_3 edge, the core hole effect is more important.[25] Since Ce is not in the tetravalent state in the alloys under study,[5] one does not need to take into account many-body effects like in the case of tetravalent Ce in CeO_2.[25]

III. RESULTS AND DISCUSSION

In Fig. 1, we present the experimental Fe *K*-edge XANES of $Al_{90}Fe_3Ce_7$, $Al_{90}Fe_5Ce_5$, and $Al_{90}Fe_7Ce_3$. The spectra are similar in nature. This result is expected, taking into account the small differences in the stoichiometry of these alloys.

In Fig. 2, we show a comparison of the experimental Fe *K*-edge XANES for amorphous $Al_{90}Fe_3Ce_7$ and the theoretical Fe *K*-edge XANES calculated for two binary model alloys: crystalline $FeAl_3$ and crystalline $FeAl_6$ (with actual atomic distances and those reduced by 3.4%). The theoretical XANES for both models are qualitatively similar. However, according to the energy position of peak *C* as well as the double *A*-*A'* structure, the $FeAl_6$ model with atomic distances reduced by 3.4% gives a better agreement with the experimental XANES data. Hence, we conclude that the local structure around the Fe site in *a*-$Al_{90}Fe_3Ce_7$ is close to the one deduced from crystalline $FeAl_6$ with atomic distances reduced by 3.4%. It is to be noted that the Fe-Al distance in *a*-$Al_{90}Fe_3Ce_7$ is reduced by 3.9% from that in *c*-$Al_{90}Fe_3Ce_7$ (Table I).

In Fig. 3, we present a comparison of theoretical XANES spectra calculated using structural data for the crystalline $FeAl_6$ as a function of cluster size. The calculations were made using interatomic distances for crystalline $FeAl_6$ reduced by 3.4%. Clearly, the XANES features are dominated by the contribution from the first shell of atoms (cluster size of 2.46 Å). However, expanding the cluster size to include the second and the third shells is essential in order to reproduce all of the features observed in the experimental Fe *K*-edge XANES for the amorphous alloys. While peaks *B* and *C* do not change by increasing the size of the cluster, the low-energy shoulder is split into two components: *A* and *A'*. In the low-energy region, the mean free path of the photoelectron is large and the inclusion of the multiple scattering within a large cluster of atoms around the absorbing one in the theoretical simulation is essential. Thus, the low-energy region of the XANES spectrum contains information pertinent not only to the first shell of atoms, but also to fairly distant atoms.

Another factor (beyond phase shifts and cluster local

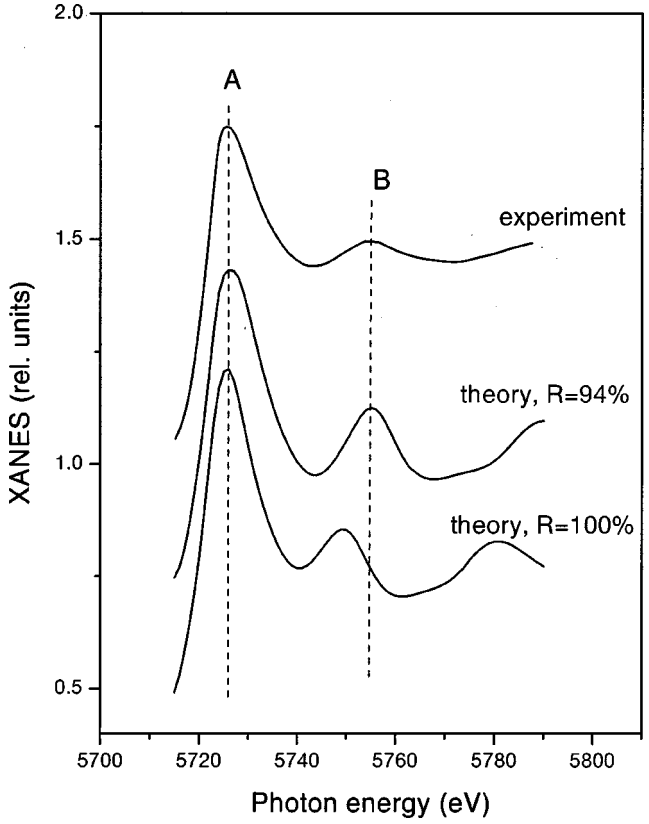

FIG. 5. Experimental Ce L_3-edge XANES for a-$Al_{90}Fe_3Ce_7$ compared with theoretical XANES calculated for crystalline $CeAl_4$ using actual distances ($R=100\%$) and those reduced by 6% ($R=94\%$).

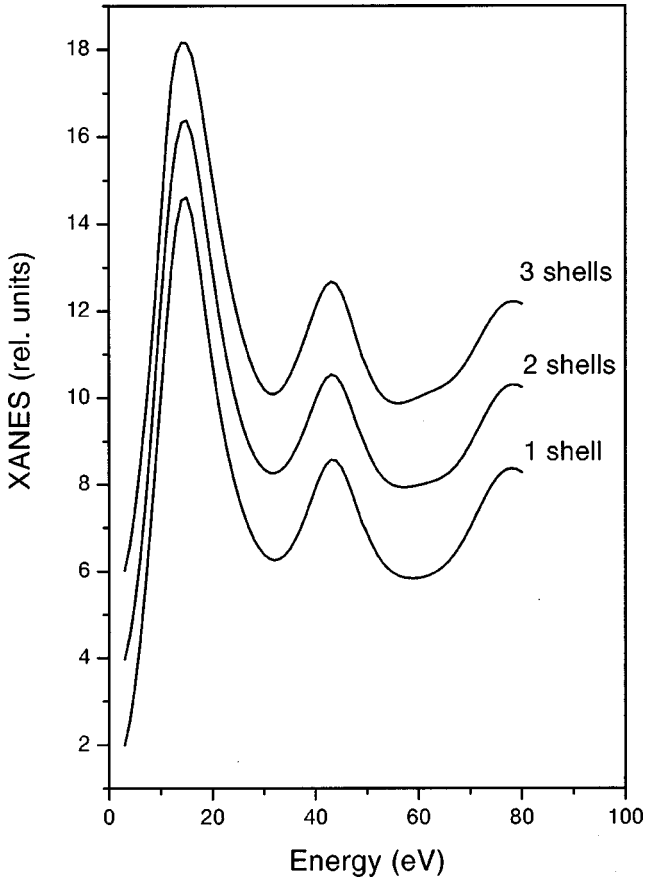

FIG. 6. Theoretical Ce L_3-edge XANES spectra calculated as a function of cluster size using structure data for crystalline $CeAl_4$ with atomic distances reduced by 6%. Origin of the energy scale corresponds to the zero of the MT potential.

structure) that determines the XANES is the transition matrix element (2) that influences the relative intensity of the XANES features. Since the energy dependence of the dipole transition matrix element is nonoscillatory in nature in the region above 30 eV from the absorption threshold, one can use the Fe *K*-edge XANES of these alloys to study the density of unoccupied Fe states with *p* symmetry in the conduction band.

In Fig. 4, we show the experimental Ce L_3-edge XANES for the amorphous alloys. Differences in the spectra of these alloys are even less pronounced than in the case of the Fe *K*-edge XANES. The similarities in the spectra are due to the narrow range of stoichiometries presented here as well as the more localized nature of the Ce *d* states in comparison with the Fe *p* states. The Ce *d* states are more atomiclike and thus less sensitive to fine details of geometry around the central absorbing atom.

A comparison of experimental Ce L_3-edge XANES of a-$Al_{90}Fe_3Ce_7$ and theoretical XANES spectra calculated using actual atomic distances for crystalline $CeAl_4$ and those reduced by 6% (Table III) is presented in Fig. 5. Clearly, the theoretical XANES spectrum calculated with interatomic distances reduced by 6% is in better agreement with the experimental XANES spectrum for a-$Al_{90}Fe_3Ce_7$. Thus, we conclude that the local structure of Ce in the amorphous alloys is better described by the local structure parameters of Ce in crystalline $CeAl_4$ with atomic distances reduced by 6%. The localized nature of the Ce *d* states is manifested in the data presented in Fig. 6 where no significant change in the theoretical XANES spectra can be realized with increasing cluster size. The main features of the XANES spectrum are realized by including only the first shell of atoms. In spite of this localization character of Ce *d* states, in some cases (like the CeO_2 system[25]), the distant atoms of the second and third shells affect the shape of the Ce L_3-edge XANES.

In Fig. 7, we present the experimental Al *K*-edge XANES spectra for the three alloys under study. The spectra are close to each other, as one expects taking into account the close stoichiometries of the alloys and the dominance of the Al component of composition. Since the signal-to-noise ratios of the spectra for the $Al_{90}Fe_7Ce_3$ and $Al_{90}Fe_3Ce_7$ alloys are significantly smaller than that of the spectrum for the $Al_{90}Fe_5Ce_5$ alloy, the theoretical analysis will be limited to the spectrum of the $Al_{90}Fe_5Ce_5$ alloy.

As in the case of the Fe *K*-edge XANES, we used two binary model alloys: crystalline $FeAl_3$ and crystalline $FeAl_6$ (with actual atomic distances and those reduced by 3.4%). For the $FeAl_6$ model compound, Al has four nonequivalent sites with relative weights (or multiplicities) of 1:2:2:1 for sites 1, 2, 3, and 4, respectively. In Table IV, we present the structure parameters for the cluster used for the calculation. The theoretical spectrum is a weighted sum of four spectra

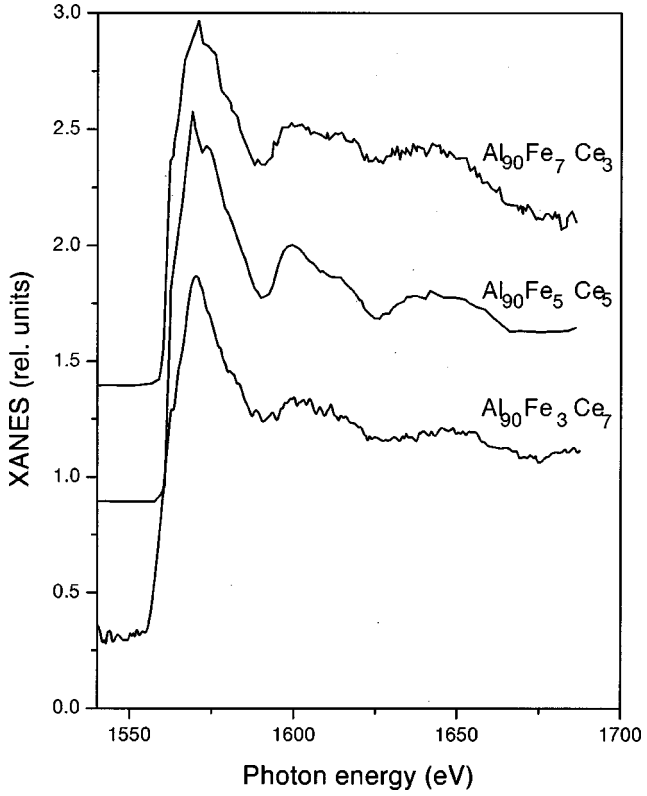

FIG. 7. Experimental Al *K*-edge XANES for amorphous $Al_{90}Fe_xCe_{10-x}$ ($x=3$, 5, and 7) alloys.

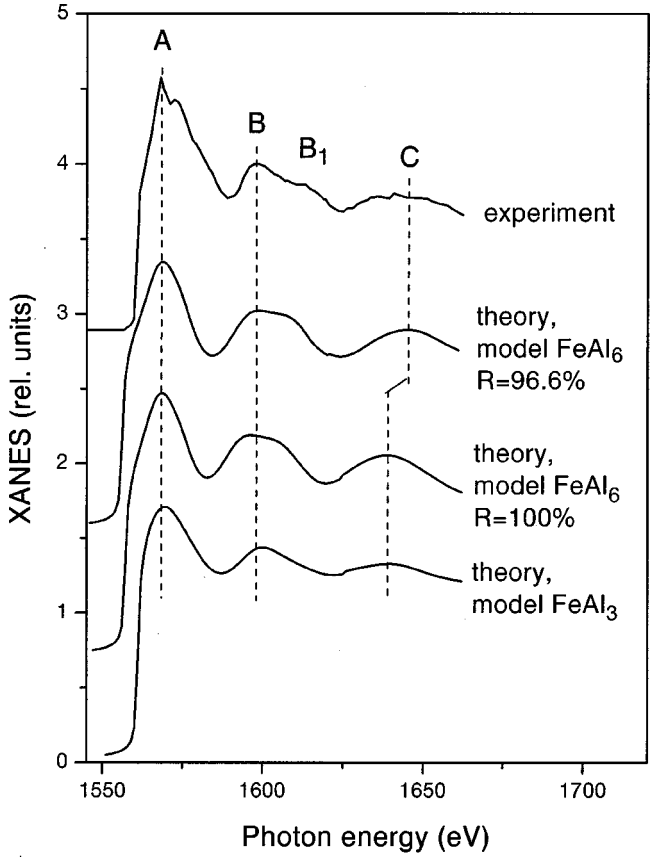

FIG. 8. Experimental Al *K*-edge XANES for amorphous $Al_{90}Fe_5Ce_5$ compared with theoretical XANES for model compounds: crystalline $FeAl_3$, pseudo-$FeAl_6$, and pseudo-$FeAl_6$ with distances reduced by 3.4%.

calculated for each of the Al sites. However, in order to get agreement with the experimental XANES spectra, especially the relative heights of the *B* and B_1 structures, the relative weights for the Al sites used in the theoretical calculation was set to 2:1:1:2. This departure from the actual relative weights for the Al sites enhances the Al-Al contributions relative to the Al-Fe contributions since the number of Al-Fe bonds for sites 1 and 4 is half that for sites 2 and 3. The enhancement of the Al-Al bonds relative to the Al-Fe bonds is essential to account for the fact that the number of Al-Fe bonds in the amorphous alloys should be smaller than the number of Al-Fe bonds in the $FeAl_6$ model since the Fe/Al ratio in the amorphous alloys is significantly less than that of the $FeAl_6$ model. Hereafter, we refer to the $FeAl_6$ model with the modified multiplicities of the Al sites as the psuedo-$FeAl_6$ model. In Fig. 8, we present a comparison of the experimental spectrum with the theoretical simulations for the above-mentioned models. As one can see, the $FeAl_3$ model gives a spectrum that does not show a split or double peak for the *B* structure as observed in the experimental spectrum and hence, can be excluded. On the other hand, the theoretical spectrum for the pseudo-$FeAl_6$ model shows a clear double-peak structure in the energy interval around 1600 eV (components *B* and B_1) in agreement with the experimental data. The energy positions of both the *B* and *C* maxima in the theoretical spectrum of pseudo-$FeAl_6$, however, differ from the experimental values. The energy positions of peaks *B* and *C* in the theoretical spectrum match the corresponding positions in the experimental spectrum only when the interatomic distances of the crystalline pseudo-$FeAl_6$ model are reduced by 3.4%. Hence, we conclude that the local geometry around

TABLE IV. Structure parameters for the four nonequivalent Al sites in crystalline $FeAl_6$ with interatomic distances reduced by 3.4% from the actual ones.

Shell number	Number and type	Shell radii (Å)
Site 1		
1	1 Fe+2 Al	2.434
2	8 Al	2.732
3	2 Al	3.278
Site 2		
1	2 Fe+2 Al	2.555
2	7 Al	2.796
3	4 Al	3.277
Site 3		
1	2 Fe+6 Al	2.590
2	3 Al	2.822
3	2 Al	3.299
Site 4		
1	1 Fe+4 Al	2.493
2	6 Al	2.824
3	2 Al	3.279

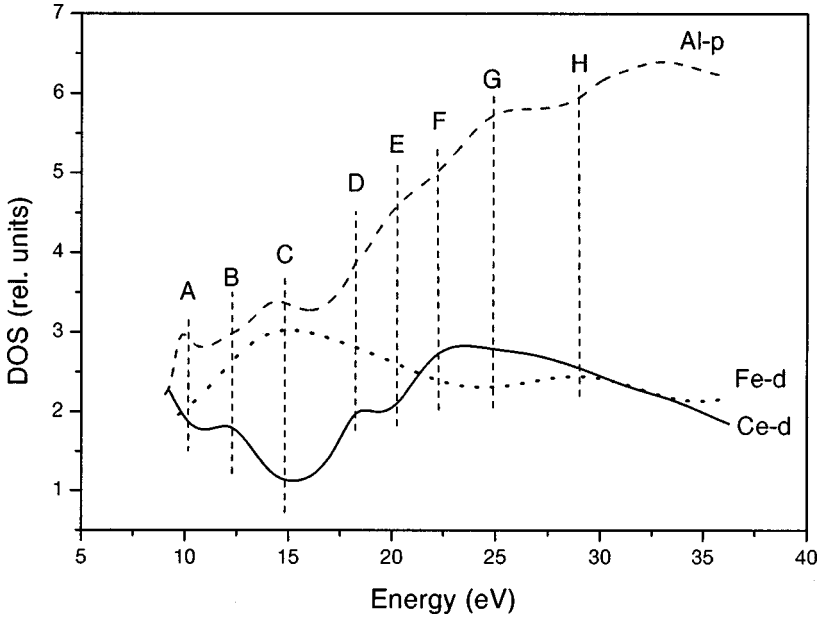

FIG. 9. Projected density of unoccupied states for the $Al_{90}Fe_xCe_{10-x}$ alloys. Origin of the energy scale corresponds to the zero of the MT potential.

the Al sites in $Al_{90}Fe_5Ce_5$ is close to that of the Al sites in the crystalline pseudo-$FeAl_6$ model with interatomic distances reduced by 3.4%.

In the energy interval up to 50 eV above the Fermi level, the value of the dipole transition matrix element for the Al *K*-edge XANES changes by a factor greater than 10. Thus, one cannot use the Al *K*-edge XANES to study the distribution of Al *p* states in the conduction band of the investigated alloys. Therefore, we have calculated the density of Al *p*-unoccupied states using the same crystal potential, which we showed provided good agreement between the theoretical and the experimental XANES. In order to study the mutual influence of the Al *p* states with the states of other atoms in the system, we also calculated the density of unoccupied Fe *d* and Ce *d* states. The results are presented in Fig. 9. In pure aluminum, electrons in the conduction band can be described in a nearly-free-electron model and their density-of-states curve is a square-root function of the energy. In the alloy under study (with 5% Fe and 5% Ce), we find a specific interaction of unoccupied Al *p* states with Fe *d* and Ce *d* states. The more localized Ce *d* and Fe *d* states push the Al *p* states from the energy interval of their maxima. As one can see in Fig. 9, the Al *p* states have minima in the energy intervals where Ce *d* (and Fe *d*) states have maxima. The only exception is in the energy interval labeled *C*, where both the Al *p* and the Fe *d* have maxima. Note that this region displays the main minimum of the most localized Ce *d* states. Thus, in the case of the Al *p* states in the $Al_{90}Fe_xCe_{10-x}$ alloys, the chemical interactions are not simple hybridization resulting in an admixture of electronic states, but a more complex phenomenon, close to the one found in the conduction band of CeO_2 (Ref. 25) and transition-metal oxides.[26] This result agrees with recent findings[27] that the addition of Ce into the $Al_{90}Fe_{10}$ alloy results in the appearance of certain covalent contributions into the chemical bond of the alloy. According to its specific features, the covalent part of the chemical bond in $Al_{90}Fe_xCe_{10-x}$ alloys increases the difficulty of crystallization and thus favors glass state formability. The possible influence of the Al *s*- and *p*-states, and transition-metal *d*-state hybridization on the stability of another Al-based system, namely, $Al_{60}Cu_{20}Co_{20}$ has been mentioned recently.[28]

IV. CONCLUSIONS

Theoretical analysis of experimental XAFS on the basis of multiple scattering has been applied to study the peculiarities of the local atomic and electronic structure of amorphous $Al_{90}Fe_xCe_{10-x}$ alloys. Results from analysis of EXAFS spectra were limited to local structure parameters of the first shell. Comparison of experimental and theoretical XANES above the Fe and Al *K* edges enabled us to determine the local structure around the Fe and Al sites up to the third shell of atoms. Comparison of experimental and theoretical XANES above the Ce L_3 edge proved that the experimental Ce XANES is dominated by contributions from the first shell of atoms. It is to be noted that the fine structure of the Fe *p* and Al *p* densities of unoccupied states in the low-energy region evolves from a large cluster, which includes at least three shells.

ACKNOWLEDGMENTS

We are thankful to Professor S.J. Poon (University of Virginia) for providing the amorphous alloys for analysis. A.N.M. acknowledges financial support by the Carderock Division of the Naval Surface Warfare Center's in-house Laboratory Independent Research Program sponsored by the ONR, administrated under program Element No. 0601152N. The support of the U.S. DOE under Contract No. DE-AS05-80-ER-10742 for its role in the development and operation of beamline X-11A at the National Synchrotron Light Source (NSLS) is also acknowledged. The NSLS is supported by the U.S. DOE under Contract No. DE-AC02-76CH00016.

*Author to whom correspondence should be addressed. FAX: (301) 227-4732. Email address: MansourAN@NSWCCD.Navy.Mil

[1] H. Y. Hsieh, B. H. Toby, T. Egami, Y. He, S. J. Poon, and G. J. Shiflet, J. Mater. Res. **5**, 2807 (1990); H. Y. Hsieh, T. Egami, Y. He, S. J. Poon, and G. J. Shiflet, J. Non-Cryst. Solids **135**, 248 (1991).

[2] G. J. Shiflet, Y. He, and S. J. Poon, J. Appl. Phys. **64**, 6863 (1988).

[3] J. L. Wagner, K. M. Wong, F. S. Pierce, and S. J. Poon, Phys. Rev. B **39**, 5500 (1989).

[4] A. N. Mansour and C. A. Melendres, J. Electrochem. Soc. **142**, 1961 (1995).

[5] A. N. Mansour, C. A. Melendres, Y. He, S. J. Poon, and G. F. Shiflet, J. Electrochem. Soc. **143**, 614 (1996).

[6] A. N. Mansour, C.-P. Wong, and R. A. Brizzolara, Phys. Rev. B **50**, 12 401 (1994).

[7] G. T. Laissardiere, Z. Dankhazi, E. Belin, A. Sadoc, N. M. Duc, D. Mayou, M. A. Keegan, and D. A. Papaconstantopoulos, Phys. Rev. B **51**, 14 035 (1995).

[8] E. Belin-Ferre, Z. Dankhazi, V. Fournee, A. Sadoc, C. Berger, H. Muller, and H. Kirchmayr, J. Phys.: Condens. Matter **8**, 6213 (1996).

[9] J. Wong, G. N. George, I. J. Pickering, Z. U. Rek, M. Rowen, T. Tanaka, G. H. Via, B. De Vries, D. E. W. Vaughan, and G. E. Brown, Jr., Solid State Commun. **92**, 559 (1994).

[10] Z. H. Levine and B. Ravel, J. Appl. Phys. **85**, 558 (1999).

[11] D. Cabaret, P. Sainctavit, P. Ildefonse, and A.-M. Flank, J. Phys.: Condens. Matter **8**, 3691 (1996).

[12] E. Sevillano, H. Meuth, and J. J. Rehr, Phys. Rev. B **20**, 4908 (1979).

[13] P. J. Durham, in *X-Ray Absorption: Principles, Applications, Techniques of EXAFS, SEXAFS, and XANES*, edited by D. C. Koningsberger and R. Prins (Wiley, New York, 1988), p. 53.

[14] T. Fujikawa, T. Matsuura, and H. Kuroda, J. Phys. Soc. Jpn. **52**, 905 (1983).

[15] D. D. Vvedensky, D. K. Saldin, and J. B. Pendry, Comput. Phys. Commun. **40**, 421 (1986).

[16] S. Della Longa, A. V. Soldatov, M. Pompa, and A. Bianconi, Comput. Mater. Sci. **4**, 199 (1995).

[17] R. V. Vedrinskii, V. L. Kraizman, A. A. Novakovich, Ph. V. Demekhin, and S. V. Urazhdin, J. Phys.: Condens. Matter **10**, 9561 (1998).

[18] J. J. Rehr and R. C. Albers, Rev. Mod. Phys. **72**, 621 (2000).

[19] A. N. Mansour, A. Dmitrienko, and A. V. Soldatov, Phys. Rev. B **55**, 15 531 (1997).

[20] Y. He, S. J. Poon, and G. J. Shiflet, Science **241**, 1640 (1988).

[21] P. Villars and L. D. Calvert, *Pearson's Handbook of Crystallographic Data for Intermetallic Phases* (American Society for Metals, Metals Park, OH, 1985), Vol. 2, pp. 920 and 972.

[22] P. J. Black, Acta Crystallogr. **8**, 43 (1955); **8**, 175 (1955).

[23] J. E. Muller, O. Jepsen, and J. W. Wilkins, Solid State Commun. **42**, 365 (1982).

[24] *Unoccupied Electronic States*, edited by J. C. Fuggle and J. E. Inglesfield (Springer, Berlin, 1992).

[25] A. V. Soldatov, T. S. Ivanchenko, S. Della Longa, A. Kotani, Y. Iwamoto, and A. Bianconi, Phys. Rev. B **50**, 5074 (1994).

[26] A. V. Soldatov, N. A. Povahzynaja, and G. E. Yalovega, Phys. Status Solidi B **195**, K1 (1996).

[27] L. Zhang, Y. Wu, X. Bian, H. Li, W. Wang, and S. Wu, J. Non-Cryst. Solids **262**, 169 (2000).

[28] R. Haerle and P. Kramer, Phys. Rev. B **58**, 716 (1998).